NIH Public Access
Author Manuscript
Acta Neuropathol. Author manuscript; available in PMC 2014 July 01.

Published in final edited form as:
Acta Neuropathol. 2013 July ; 126(1): 59–74. doi:10.1007/s00401-013-1119-4.

Mild Traumatic Brain Injury in the Mouse Induces Axotomy Primarily within the Axon Initial Segment

John E. Greer[1], **Anders Hånell**[1], **Melissa J. McGinn**[1], and **John T. Povlishock**[1]
[1]Department of Anatomy and Neurobiology, Virginia Commonwealth University School of Medicine

Abstract

Traumatic axonal injury (TAI) is a consistent component of traumatic brain injury (TBI), and is associated with much of its morbidity. Increasingly it has also been recognized as a major pathology of mild TBI (mTBI). In terms of its pathogenesis, numerous studies have investigated the susceptibility of the nodes of Ranvier, the paranode and internodal regions to TAI. The nodes of Ranvier, with their unique composition and concentration of ion channels, have been suggested as the primary site of injury, initiating a cascade of abnormalities in the related paranodal and internodal domains that lead to local axonal swellings and detachment. No investigation, however, has determined the effect of TAI upon the axon initial segment (AIS), a segment critical to regulating polarity and excitability. The current study sought to identify the susceptibility of these different axon domains to TAI within the neocortex, where each axonal domain could be simultaneously assessed. Utilizing a mouse model of mTBI, a temporal and spatial heterogeneity of axonal injury was found within the neocortical gray matter. Although axonal swellings were found in all domains along myelinated neocortical axons, the majority of TAI occurred within the AIS, which progressed without overt structural disruption of the AIS itself. The finding of primary AIS involvement has important implications regarding neuronal polarity and the fate of axotomized processes, while also raising therapeutic implications, as the mechanisms underlying such axonal injury in the AIS may be distinct from those described for nodal/paranodal injury.

Keywords

diffuse axonal injury; traumatic brain injury; axon initial segment

Introduction

It is well recognized that traumatic axonal injury (TAI), commonly termed diffuse axonal injury (DAI) in humans, is a consistent feature of a traumatic brain injury (TBI) and is believed to be a major contributor to its subsequent morbidity [26, 38, 39, 54, 70]. This fact has been affirmed in multiple studies performed in experimental models of injury as well as human post mortem examinations, in which the occurrence of axonal injury has been identified across the spectrum of human TBI ranging from mild through severe [26, 52, 38, 39, 54]. Further, through the use of modern imaging, the importance of DAI has also been confirmed in humans wherein diffusion tensor imaging has consistently identified white

Corresponding Author: John T. Povlishock, Department of Anatomy and Neurobiology, Virginia Commonwealth University, P.O. Box 980709, Richmond, Virginia 23298-0709, Phone: 804-828-9623, Fax: 804-828-9477, jtpovlis@vcu.edu.
Mailing address for all authors: Department of Anatomy and Neurobiology, Virginia Commonwealth University, P.O. Box 980709, Richmond, Virginia 23298-0709

Conflict of Interest
The authors declare that they have no conflict of interest.

NIH-PA Author Manuscript
NIH-PA Author Manuscript
NIH-PA Author Manuscript

NIH-PA Author Manuscript

NIH-PA Author Manuscript

NIH-PA Author Manuscript

matter tracts exhibiting reduced fractional anisotropy, the hallmark of DAI, in individuals who have sustained traumatic injuries [4, 6, 26, 39, 59, 67]. More recently, the use of susceptibility-weighted imaging has also confirmed the occurrence of TAI even following mild injury [78]. While the importance of TAI /DAI cannot be disputed, limitations exist in our understanding of its precise initiating pathogenesis in the traumatically perturbed brain parenchyma.

Although multiple *in vivo and in vitro* studies have shown that traumatic initiation of focal alterations in axolemmal permeability and/or local channelopathy result in the dysregulation of intra-axonal calcium, mitochondrial damage, and the activation of damaging cysteine protease cascades that disrupt axonal transport and cause local axonal swelling and detachment [70], no consensus exists as to the precise point along the axon's length that this damaging cascade is initiated. In the myelinated axonal population, various lines of evidence suggest the involvement of nodal [18, 44, 42, 45] as well as paranodal and internodal sites [16, 49, 56]. However, no information exists on the potential involvement of the axon initial segment (AIS) or its predilection for initiating reactive axonal change. This issue is of more than academic interest in that involvement of the initial axonal segment versus nodal and paranodal segments could pose different mechanistic issues relevant to the subsequent pathogenesis of the induced axonal change, its functional correlates, and its potential therapeutic modification. The failure of the research community to make progress in this key area has not resulted from a lack of effort. Rather, it stems from the lack of investigative tools required to identify with a high degree of fidelity, the precise site of axonal injury within minutes of the traumatic event. Specifically, most studies conducted to date have relied on immunohistochemical approaches to identify impaired axonal transport or cytoskeletal disruption and/or the activation of cysteine protease cascades, all of which reflect the early sequelae of axonal injury, while not necessarily delineating their anatomical site of origin.

Recently, we characterized a model of mTBI using transgenic mice expressing yellow fluorescent protein within scattered neurons of Lamina V of the neocortex. Using this transgenic mouse line, we followed with fidelity, the chronic progression of traumatically-induced axonal injury and its consequences for the sustaining cell bodies of origin together with the subsequent reorganization of the retained axonal segment [20]. Appreciating the uniqueness of this model system for following the chronic sequelae of DAI, we also recognized that these same YFP-expressing neurons could provide a platform on which to identify, with precision, the site of initial axonal injury based upon subtle alterations in the intra-axonal YFP pooling and swelling. To improve the fidelity of site recognition, we also appreciated that the use of contemporary markers of paranodal alignment, targeting contactin-associated protein (Caspr) expression, offered additional benefit in determining if these initiating axonal changes localized to either the nodal, internodal or the initial segment domains.

In the current study, we utilized the above-described transgenic YFP expressing mice together with Caspr immunoreactivity to define within the neocortex those sites most commonly linked to the initiation of axonal injury. Using confocal analyses interfaced with both a qualitative and quantitative evaluation, we demonstrate that the initiation of axon swelling occurs not only at the nodal and paranodal domains, but also at the AIS which showed a predilection for traumatically induced axonal damage within the neocortex. Moreover, within the AIS, the reactive axonal change was highly focal, with only subtle alteration of the remaining segment.

NIH-PA Author Manuscript

NIH-PA Author Manuscript

NIH-PA Author Manuscript

Material and Methods

The Thy1-YFP-H line [B6Cg-TgN(Thy1-YFP-H)2Jrs, stock number 003782] was obtained from the Jackson Laboratories (Bar Harbor, ME) and maintained as heterozygotes upon a C57BL/6J background. Inheritance of the fluorescent transgene was determined from an ear punch taken at weaning (approximately 21d). The tissue from the ear punch was mounted on a glass slide and examined using a FITC filter on an Olympus DP71 digital camera (Olympus, Center Valley, PA) where YFP^+ axons could easily be identified in animals carrying the YFP transgene. YFP expression in these mice is under the control of the neuronal specific Thy1 promoter, resulting in YFP expression within the neocortex that is primarily restricted to Layer V pyramidal neurons [17].

Mild central fluid percussion injury (cFPI) was induced as described previously utilizing YFP-H mice [20, 21]. Briefly, 35 YFP-H male mice, 8–10 weeks old, weighing 20–26 grams were surgically prepared for the induction of cFPI. Each animal was anesthetized in an anesthesia chamber with 4% isoflurane in 100% O2. After induction, animals were placed in a stereotactic frame (Stoelting, Wood Dale, IL) fitted with a nose cone to maintain anesthesia with 1–2% isoflurane in 100% O2. A thermostatically controlled heating pad (Harvard Apparatus, Holliston, MA) was then placed under the animal and set to monitor the rectal temperature and, via feedback control, maintain the body temperature at 37°C during the surgery. A midline sagittal incision was made to expose the skull from bregma to lambda. The skull was cleaned and dried and a 3.0 mm circular craniotomy was then made along the sagittal suture midway between bregma and lambda, leaving the underlying dura intact. A sterile Leur-Loc syringe hub was then cut away from a 20-gauge needle, and affixed to the craniotomy site using cyanoacrylate. Upon confirming the integrity of the seal between the hub and the skull, dental acrylic was then applied around the hub to provide stability during the induction of injury. After the dental acrylic hardened, the scalp was sutured around the hub, topical bacitracin and lidocaine ointment were applied to the incision site, and the animal was removed from anesthesia and monitored in a warmed cage until fully ambulatory (approximately 60–90 minutes). For the induction of injury, each animal was re-anesthetized with 4% isoflurane in 100% O2, and the male end of a spacing tube was inserted into the hub. The female end of the hub- spacer assembly, filled with 0.9% saline, was attached on to the male end of the fluid percussion apparatus (Custom Design & Fabrication; Virginia Commonwealth University; Richmond, VA). An injury of mild severity (1.7±0.04 atmospheres) was administered by releasing a pendulum onto a fluid-filled piston to induce a brief fluid pressure pulse upon the intact dura. The pressure pulse measured by the transducer was displayed on a storage oscilloscope (Tektronix 5111, Beaverton, OR), and the peak pressure was recorded. After injury, the animals were visually monitored for recovery of spontaneous respiration. The hub and dental acrylic were removed en bloc, and the incision was rapidly sutured before recovery from anesthesia/ unconsciousness. Topical bacitracin and lidocaine were then applied to the closed scalp incision. The duration of transient unconsciousness was determined by measuring the time it took each animal to recover the following reflexes: toe pinch, tail pinch, corneal blink, pinnal, and righting. After recovery of the righting reflex, animals were placed in a warmed holding cage to ensure the maintenance of normothermia and monitored during recovery before being returned to the vivarium. For animals receiving a sham injury, all of the above steps were followed with the exception of the release of the pendulum to induce the injury. The Virginia Commonwealth University School of Medicine Institutional Animal Care and Use Committee approved all animal procedures.

Following injury, animals were allowed to recover for times ranging from 3–4 min to 12 hours post injury (sham, n=12; 3–4m, n=2; 15m, n=4; 1h, n=5; 3h, n=3; 6h, n=6; 12h, n=3) at which time they were intraperitoneally injected with an overdose of sodium pentobarbital

NIH-PA Author Manuscript

NIH-PA Author Manuscript

NIH-PA Author Manuscript

and then transcardially perfused with heparinized normal saline followed by 4% paraformaldehyde in Millonig's buffer. After perfusion, the occipital and parietal bones were removed and the brain and remaining skull were immersed in the perfusion fixative for 24h at 4°C. Each brain was then removed from the skull and blocked coronally at the optic chiasm and the midbrain to include the parietal and temporal cortices, hippocampus, and thalamus. Blocked brains were flat mounted with cyanoacrylate, embedded in agar and 40μm free-floating coronal serial tissue sections were cut using a vibratome (Leica VT1000S; Leica Microsystems, Bannockburn, IL). Sections were collected from −0.58mm to −2.5mm posterior to bregma, for a total of 48 sections. The tissue was stored in Millonig's buffer in 24-well culture plates until further use (Falcon, Newark, DE).

Allocated sections were then processed with antibodies targeting β-APP (1:500), an established marker of axonal damage [65, 66, 19, 8, 74, 9, 34–36, 47, 48, 40, 37, 29] that permitted comparison of these immunoreactive profiles to those identified through the endogenous YFP expression. Additionally, antibodies targeting the cytoskeletal proteins, contactin-associated protein (Caspr) (1:200) and ankyrin-G (1:200), were employed utilizing immunohistochemical techniques described previously [20]. As noted previously, anti-Caspr antibodies were utilized to identify paranodal, nodal and axon initial segment domains along a single axon's length. Caspr, a member of the neurexin protein family, along with other cell adhesion molecules is responsible for the development and maintenance of the paranodal junctions, and the association between the terminal loops of the myelin with the paranode of the axon [55]. Caspr immunoreactivity, which is distributed along the myelinated axon's length, forms immunoreactive bands flanking the nodes of Ranvier with a single $Caspr^+$ band, delineating the para-AIS, where the myelin sheath first establishes axonal contact. Thus, in addition to marking paranodal/nodal regions it also serves as a marker delineating the para-AIS, the more proximal AIS domain and the more distal juxtapara-AIS [15]. Furthermore, antibodies to ankyrin G were used to assess AIS cytoskeletal integrity to determine if DAI initiated only focal change versus a more expansive disruption of the AIS.

Routine fluorescent image acquisition and quantitative analyses

For quantitative analysis a random well was selected (1–24) and 2 coronal tissue sections from each case, 240 μm apart, were selected for immunolabeling for Caspr (6–8 coronal sections were utilized for the 3m post-injury time point due to a paucity of swellings at this time point). Within each section all YFP^+ neurons within Layer V with associated axonal swellings were identified throughout the entire neocortex, bilaterally. A total of 274 axonal swellings were analyzed at the following post-injury time points: 3m (n=1), 15m (n=49), 1h (n=65), 3h (n=57), 6h (n=63) and 12h (n=39). A blinded investigator performed all quantitative analyses. The remaining tissue sections were processed for qualitative immunofluorescent analysis. Quantitative fluorescent microscopic analyses and image acquisition were performed using a Nikon Eclipse 800 microscope (Tokyo, Japan) fitted with an Olympus DP71 digital camera (Olympus, Center Valley, PA) with the appropriate excitation/emission filters.

Quantification of swelling size

Utilizing routine fluorescent microscopy and a l00× objective lens, axonal swellings were identified along the length of YFP^+ axons within Layer V throughout the neocortex bilaterally. For each swelling the length and diameter were measured utilizing a micrometer fitted within the microscope eyepiece. Swelling length was determined by measuring from the region of disconnection to the portion of non-dilated axon proximal to the swelling of interest. For swellings along continuous axons, length was measured between the two regions of non-dilated axon related to the focal swelling. For each injured axon, additional information was collected. The number of axons with multiple swellings and the number of

NIH-PA Author Manuscript

NIH-PA Author Manuscript

NIH-PA Author Manuscript

axons demonstrating a focal swelling yet retaining continuity with the distal axonal segment at each given time point were quantified.

Quantification of swelling location relative to axon domains

To determine the location of YFP^+ swellings relative to specific initial, nodal, paranodal and internodal axon domains, swelling location relative to Caspr immunoreactivity was determined. Briefly, utilizing routine fluorescent microscopy and a 40× and 100× objective lens, swellings were identified along the length of YFP^+ axons within Layer V throughout the neocortex bilaterally. $Caspr^+$ immunolabeling of YFP^+ axon in sham, uninjured animals consisted of pairs of $Caspr^+$ paranodes distributed on the YFP^+ axon, allowing for identification of the paranodal and nodal regions. At the distal end of the initial segment, however, Caspr immunoreactivity was limited to a single band, reflecting the presence of what has been termed the para-AIS [15]. This $Caspr^+$ para-AIS domain was subsequently utilized to identify traumatically induced swellings within the proximally oriented AIS as well as swellings within the para-AIS/juxtapara-AIS domains.

Briefly, YFP^+ axonal swellings, in which continuity could be established with the cell body of origin, were identified throughout Layer V within the neocortex, bilaterally. Once identified, they were classified based upon their location relative to $Caspr^+$ immunoreactive domains, as: 1. nodal swellings, those swellings located between two Caspr paranodes; 2. paranodal/juxtaparanodal swellings, located either within or adjacent to Caspr paranodes; 3. internodal swellings, located along the axon between two $Caspr^+$ paranodal/nodal regions, 4. swellings within the AIS and last 5. swellings within the para-AIS and/or juxtapara-AIS regions.

Confocal Microscopy

Images of axotomized YFP^+ neurons colabeled with antibodies targeting APP, Caspr and ankyrin-G were acquired with both a Leica TCS-SP2 AOBS and a Zeiss LSM 700 confocal microscope. Images presented are z-axis projections compiled utilizing ImageJ (NIH). A sequential scan was utilized to eliminate the potential for crosstalk between the YFP fluorophore and Alexa dyes utilized for immunolabeling.

Data Analysis

Quantitative data concerning swelling length, diameter, axon continuity and swelling location was tested for significance using an one way analysis of variance followed by a LSD posthoc analysis with $p<0.05$ considered statistically significant. No significant changes in the location of axonal swellings were noted between different time points post-injury and values presented are averages from all the different time points. All results are presented as the mean ± standard error.

Results

General Pathophysiologic Findings

Mild cFPI in mice induced a transient suppression of the righting reflex in all injured animals of 8.8±0.5 min that was significantly longer than that of 1.9±0.2 min resulting from sham injury ($p<0.05$). The 2 min righting reflex for sham animals is consistent with recovery from the surgical plane of anesthesia induced by 4 min of 4% isoflurane and does not reflect recovery from sham-injury. Further, no significant difference in righting reflex suppression was noted between injury groups ($p> 0.05$), indicating that all groups received injuries of comparable severity. No hind limb seizures were noted in any animals, though transient apnea was observed in several animals following injury. This apneic episode was of short duration (<1 min) and resolved spontaneously without intervention.

NIH-PA Author Manuscript

NIH-PA Author Manuscript

NIH-PA Author Manuscript

Early Axonal Injury in YFP-H Mice

Consistent with previous studies utilizing the YFP-H transgenic strain of mice [13, 75], YFP^+ neurons in the neocortex of injured and sham-injured control animals were observed primarily within Layer V, though isolated, scattered YFP^+ neurons could also be observed within more superficial neocortical layers. Following sham-injury no YFP^+ axonal swellings or irregularities, indicative of axonal damage, were observed in the neocortex or the underlying subcortical white matter (SCWM). Axons arising from YFP^+ pyramidal neurons in sham-injured animals were continuous and could be routinely followed from their neuronal cell body of origin in Layer V into the underlying SCWM. Following injury, all tissue sections processed for YFP visualization, as well as parallel immunohistochemical analyses, revealed a pattern of macroscopic and microscopic change consistent with that routinely described in rat and mouse cFPI models of mild to moderate severity [14, 20, 69]. The dorsal neocortex showed no evidence of contusion or cavitation. The brain parenchyma itself was devoid of overt hemorrhage, with only isolated petechial hemorrhages observed in the corpus callosum. Limited subarachnoid bleeding was found over the dorsal convexity incident to the site of injury, however beyond this focus of subarachnoid hemorrhage there was no involvement of the subarachnoid compartment. At all survival times, the ventricular system maintained a normal appearance with no obvious trauma-induced ventricular enlargement.

Despite this preservation of brain parenchymal integrity typical of a mild diffuse TBI, the forces of injury consistently evoked YFP^+ axonal swellings consistent with TAI. Comparable to previous reports [20] small axonal swellings could be observed within Layer V of the neocortex, often in continuity with their cell bodies of origin. As early as 15m post-injury small swellings, ~l–2μm in diameter, (Figure 1a–c) could be identified scattered throughout the neocortex, predominantly within Layers V and VI, with the sustaining cell bodies located within Layer V. Often multiple YFP^+ axonal swellings could be observed along continuous YFP^+ axons (Figure 1c), presumably demonstrating a progressive stage prior to eventual axon disconnection. Though most swollen axons, whether containing one or several swellings, at this early time point maintained continuity with their distal axonal segments, some axons with swellings demonstrated a lack of continuity with the distal axonal segment (Figure 1b) suggesting rapid disconnection. Importantly, quantitative analysis of sections from animals sacrificed 3–4 min post-injury revealed only an isolated axonal swelling, in which no evidence for axonal disconnection was identified (Figure 1d), suggesting that the finding of early axonal swellings and their subsequent disconnection within the first 15m following injury was not a direct consequence of the primary insult, but rather, occurred progressively over a relatively rapid time course.

At the later time points of 3h, 6h and 12h post-injury, (Figure 2) the majority of axonal swellings had expanded in size (Figure 2a, b) and, in large part, had progressed to disconnection. Underscoring the heterogeneous temporal progression to disconnection, a limited number of injured axons demonstrated continuity at 3h (Figure 2c), 6h (Figure 2d) and 12h (Figure 2e), illustrating that progression from initial injury to eventual axon disconnection is variable.

Though some temporal heterogeneity existed, quantitative assessment of the integrity of swollen axons revealed a significant decrease in the percentage of swollen YFP^+ fibers maintaining axonal continuity as early as 1h post-injury (Figure 3a). At this time point, the percentage of injured axons demonstrating axonal continuity was significantly reduced to 31.1±0.1% in comparison to the 57.8±0.1% observed in continuity at 15m post-injury ($p=0.033$). The percentage of injured, yet intact axons was similarly decreased at subsequent time points (Figure 3a).

NIH-PA Author Manuscript

NIH-PA Author Manuscript

NIH-PA Author Manuscript

In addition to continuity, a quantitative assessment of the temporal changes in axonal swelling size demonstrated a significant and progressive increase in the length and width of YFP^+ swellings (Figure 3b, c). Average swelling length (Figure 3b) at 15m and 1h was found to be 2.74±0.45μm and 4.56±0.34μm, respectively. At 3h post-injury swelling length had significantly increased to 6.59±0.41μm ($p<0.01$ compared to 15m post-injury). Axon swelling length continued to increase significantly with respect to time with swelling length at 6h and 12h reached 10.12±0.47μm and 10.92±1.45μm ($p=0.028$ and $p<0.01$, respectively, as compared to 3h post-injury). No significant increase in swelling length was noted between 6h and 12h post-injury.

Following a similar progression, and reflecting enlargement of axonal swellings over time, swelling width increased significantly (Figure 3c) as early as 1h post-injury (2.62±0.18μm) when compared to swelling width observed at 15m post-injury (1.85±0.16μm) ($p<0.001$). Continued expansion was reflected in a significantly increased swelling diameter at 3h post-injury to 4.01±0.31 urn ($p=0.019$), with further significant increases at 6h post-injury (4.98±0.04μm) ($p=0.018$), beyond which time, no further radial enlargement was observed.

APP Immunohistochemistry

Consistent with previous reports following cFPI in rats [29, 30, 69] and in mice [20], focal YFP^+ axonal swellings were APP immunoreactive throughout the time course assessed (Figure 4). APP immunoreactivity was present even in the smallest swellings detected at 15m post-injury (Figure 4a, b) with continued APP accumulation as YFP^+ swellings enlarged over time (Figure 4c, d). Consistent with previous reports, sham-injured animals demonstrated no visible labeling of APP+ axonal swellings at any post-injury time point evaluated (data not shown).

As noted previously, as early as 15m following injury (Figure 1c) and continuing throughout the time course assessed, some axonal swellings occurred at multiple sites along the same YFP^+ fiber (Figure 4e–h). The number of fibers with multiple swellings did not change significantly with respect to time post-injury, constituting approximately 1/3 of the injured fibers throughout the 12h time course. Within these continuous YFP^+ fibers demonstrating multifocal swellings at early time points post-injury, APP^+ immunoreactivity was typically confined to only the most proximal swelling (Figure 4e, f). As noted, progression to disconnection was consistently observed at later time points post injury, and consistent with previous reports [20, 76], following disconnection APP immunoreactivity was typically found only within the proximal swellings (Figure 4g, h). Among this population of YFP^+ axons demonstrating multifocal axonal swellings, the majority demonstrated APP accumulation in one swelling, typically the swelling proximal to the site of axonal disconnection (Figure 4i, j), suggesting APP accumulation marks the eventual site of disconnection when multiple swellings are present.

Localization of TAI-induced axonal swellings

To localize the above-described axonal swellings with respect to specific axon domains, an anti-Caspr labeling strategy was employed. In the sham-injured animals, multiple $Caspr^+$ axoglial interactions were observed (Figure 5b, c) located along the length of single YFP^+ axons (Figure 5a). The presence of paired $Caspr^+$ immunoreactive bands flanked the nodes of Ranvier while a single $Caspr^+$ para-AIS region was localized more proximally, demarcating the end of the AIS, proximally (Figure 5).

With brain injury, traumatically induced YFP^+ axonal swellings were localized by the parallel use of $Caspr^+$ immunostaining to the nodes of Ranvier (Figure 6a–h; white arrowheads), paranodal regions (Figure 6h–m; white arrows), internodal axon segments

NIH-PA Author Manuscript

NIH-PA Author Manuscript

NIH-PA Author Manuscript

(Figure 6e–g; yellow arrowheads), the para-AIS and the AIS (Figure 7) at all time points following injury. Within many YFP^+ axons, multiple swellings were observed (Figure 6a–h), as noted previously. When multifocal swellings were found they often localized to both the nodal and paranodal regions (Figure 6a–d), consistent with nodal axonal damage and the subsequent accumulation of axoplasm within the paranode. Less frequently, internodal swellings accompanied by nodal swellings were also observed (Figure 6g–i). Paranodal swellings in the absence of nodal swellings were also observed along some intact axons (Figure 6k–m). Disconnected axons often demonstrated a single locus of $Caspr^+$ immunoreactivity that surrounded the distal tip of the swelling (Figure 6h–j), indicating axon disconnection in the nodal region. In addition to these swellings localized at the nodes of Ranvier, as well as the paranodal and the internodal segments, a large number of axonal swellings also localized to the AIS and the adjacent para/juxtapara-AIS domains (Figure 7). As early as 15m post-injury, small (2–5μm) swellings were observed both within the AIS some distance proximal to the $Caspr^+$ para-AIS (Figure 7a–c) and at the termination of the AIS, directly adjacent to the para-AIS (Figure 7d–f). Clear evidence of the evolution of early swellings which occurred within the AIS could be seen at 12h post-injury, with no evidence for $Caspr^+$ immunoreactivity within the proximal axonal segment following disconnection, though the $Caspr^+$ para-AIS was retained within the distal, disconnected axonal segment (Figure 7g–i; arrows). In addition to focal swellings and/or disconnection within the AIS, multiple axons demonstrated swellings within the para-AIS and juxtapara-AIS domains (Figure 7j–o). These swellings were found to involve both the para-AIS (Figure j–I) and the juxtapara-AIS (Figure 7m–o).

Following this qualitative evaluation, the distribution of swellings within each respective axon domain was quantified. Although this analysis revealed no change in swelling location with respect to time, the majority of YFP^+ swellings occurred within the AIS (Figure 7p), indicating that this axon domain is particularly vulnerable to the biomechanics of diffuse brain injury. Specifically, a total of 59.9% of YFP^+ swellings were located close to the cell body either within AIS (50.4%) or the para-AIS/juxtapara-AIS (9.5%) regions, while the remaining YFP^+ swellings associated with the nodes of Ranvier (18.0%), the paranodal/juxtaparanodal regions (14.4%) or the internode (7.6%). Additionally, at 15m post-injury, within the axonal population demonstrating swellings associated with the AIS or para-AIS, two-thirds of the YFP^+ axonal swellings within the AIS were located adjacent to the $Caspr^+$, para-AIS (Figure 7d–f). The remaining one-third of AIS swellings occurred within the AIS (Figure 7a–c). These results demonstrate a particular susceptibility of the AIS and para-AIS to diffuse traumatic axonal injury.

The Preservation of AIS Cytoskeletal Integrity following TAI

Because of the predilection for axonal damage within AIS, we capitalized on this localization, together with information existing on the genesis of TAI in terms of cytoskeletal disruption to determine what relation if any these AIS alterations have to one of its major cytoskeletal constituent, ankyrin G. Given the vast literature demonstrating cytoskeletal degradation [3, 63, 64, 12, 11, 25, 10, 46, 60] and rapid retrograde axonal degeneration [76] following injury, the integrity of cytoskeleton of the AIS was evaluated utilizing antibodies targeting ankyrin-G (ankG), a cytoskeletal protein whose axonal distribution is restricted to the AIS and the nodes of Ranvier. Consistent with previous reports [62], ankG antibodies consistently labeled the AIS throughout the neocortex (Figure 8a–c). Importantly the AIS of YFP+ neurons within sham-injured animals were clearly delineated by ankG expression (Figure 8d–e). At early time points post-injury, the AIS cytoskeleton within the majority of injured axons remained intact (Figure 8f, g). Within injured axons, the ankG cytoskeleton appeared intact in proximal regions of the AIS, only demonstrating focal loss of expression in relation to the site of axonal swelling. (Figure 8j,

NIH-PA Author Manuscript

NIH-PA Author Manuscript

NIH-PA Author Manuscript

k). Within isolated AIS segments some evidence of subtle cytoskeletal disruption, reflected in diminished ankG immunoreactivity, was sometimes observed (Figure 8h, i). At later time points post-injury, cytoskeletal ankG immunoreactivity was retained within the AIS proximal to the axonal swelling and this was a common finding in the many YFP^+ neurons demonstrating AIS swellings (Figures 8j–k). Importantly, even within several dilated initial segments seen at 12h post-injury, ankG immunoreactivity persisted within the axonal cylinder (Figure 8l, m), consistent with its continued integrity.

Discussion

The results of the current communication provide a detailed description of the spatiotemporal changes associated with TAI within the neocortex following diffuse TBI. Utilizing a YFP-expressing transgenic mouse model of TBI, the current manuscript provides unique insight into the axonal sites associated with the initiation of TAI. The current study's demonstration of YFP^+ swellings adjacent to intact, unaltered axons is consistent with the scattered/DAI described previously in both animals and humans [1, 51, 71]. Additionally, our quantitative evidence for the continuous enlargement of axonal swelling is also consistent with previous reports on the morphological progression of axon swelling following TAI, a finding consistent with the fact that TAI involves progressive change. In the current study, progressive linear and radial expansion of the swelling occurred between 15m and 3–6h post-injury, after which swelling size was stable. This likely reflects either an interruption of further anterograde axonal transport or a conversion of anterograde to retrograde axonal transport from the swelling [41, 61, 72, 73, 7], consistent with early reorganization and recovery of the proximal axonal segment previously reported [20].

Importantly, in contrast to previous reports, the observed temporal progression from initial, primary injury to eventual axon disconnection varied markedly. The initiation of axonal swellings at 15 min following injury is consistent with previous descriptions of swelling formation in the brainstem [43, 45, 50, 53]. However, importantly, in the current study over 40% of injured axons at 15 min demonstrated disconnection in contrast to previously published studies reporting disconnection occurring over a period of several hours post-injury [43, 45, 50, 53]. In the current study, confirmation that such rapid axon disconnection was secondary and progressive came from our failure to detect any overt axonal disconnection immediately, 3–4 min following injury. Such rapid axon disconnection is consistent with the qualitative observations of Kelley and colleagues, following TAI in the thalamus, where the majority of APP^+, swollen axons demonstrated evidence for disconnection by 30m following injury [29]. This rapid, yet progressive disconnection in a large percentage of TAI fibers has critical implications when considering therapeutic strategies targeting the multiple pathological processes attributed to secondary axonal injury, as many axons may progress to disconnection rapidly thereby limiting any potential neuroprotective strategies without the use of additional approaches aimed at extending the therapeutic window. This important observation, however, does require validation in higher order animals where the progression to disconnection may be slower [70].

In addition to the observed rapid axonal disconnection, a parallel contribution of the current study, was the finding that this axonal injury occurred within multiple domains along YFP^+ axonal fibers, including the node of Ranvier, the paranode/juxtaparanode region, the internode and, importantly, the AIS. To our knowledge, the current manuscript represents the first description of TBI-induced axonal swellings in the AIS. TAI-linked nodal injury with the formation of nodal "blebbing" has been described in various experimental models of TAI [18, 44, 42]. *In vitro* studies utilizing axonal stretch injury have demonstrated injury-induced alterations to voltage-gated sodium (VGSCs), which are known to be enriched within nodes of Ranvier [27, 58, 77]. This led to the suggestion that the node of Ranvier

NIH-PA Author Manuscript

NIH-PA Author Manuscript

NIH-PA Author Manuscript

exclusively represents the initial site of pathology and subsequent axon failure [42]. The results of the current communication suggest axonal injury can occur along the length of an individual myelinated axon. Specifically, YFP^+ swellings could be observed as early as 15m post-injury and extending throughout the time course of study within nodal, paranodal and internodal domains, consistent with previous reports of TAI in the brainstem of cats subjected to diffuse brain injury, wherein axonal injury was found to occur within all three domains [16, 49]. Additionally, these findings are also consistent with both paranodal and nodal damage described following cFPI in the rat [56]. Collectively, these findings, along with those of the current manuscript, suggest that TAI affects multiple domains within myelinated fibers in a heterogeneous fashion.

However, despite the above discussed nodal and paranodal changes described in primarily in the brainstem, it remains to be determined if parallel initial segment involvement is also found within these brainstem sites. Further it remains to be determined if AIS involvement constitutes a feature of subcortical and/or thalamic projection neurons. Importantly, although present in all domains, YFP^+ swellings found in the current study were unevenly distributed, with the majority found to occur within the AIS or para-AIS, with 60% of all YFP^+ swellings occurring therein, suggesting a predilection for injury within these specialized axonal domains. Multiple lines of evidence suggest that several of the mechanisms long associated with TAI in white matter tracts, such as axolemmal mechanoporation and sodium channel dysfunction, appear to have a limited role in TAI within the AIS raising new questions regarding its pathogenesis. Injury within the perisomatic domain of rats, now recognized to represent injury within the AIS, has not been linked to mechanoporation as evidenced by the lack small molecular weight tracer uptake [68, 29, 33]. Further, while sodium channel dysfunction, specifically cleavage of its α-subunit has been demonstrated following *in vitro* axonal stretch [27, 58, 57], both nodes of Ranvier and the distal AIS contain Navl.6 voltage-gated sodium channels, suggesting an equivalent susceptibility to VGSC proteolysis and subsequent axonal injury that was not observed in the current study.

In support of a diminished role for mechanoporation or channelopathy and subsequent Ca^{2+} dysregulation, is the relative stability of the AIS cytoskeleton observed in the current communication. Unlike previous reports demonstrating calcium and calpain-dependent complete dissolution of the ankyrin-G cytoskeleton within 3h of an ischemic insult [62], calcium-mediated calpain activation appears to play a limited role in axonal injury within the AIS, as previous studies demonstrated calpain-mediated αII-spectrin proteolysis (CMSP) within the neocortex to be primarily restricted to the gray-white matter interface at 3h and 6h post-injury [46]. These swellings are remote from the AIS of Layer V and are consistent with the nodal and paranodal swellings described in the current manuscript, further supporting the hypothesis that injury mechanisms may differ depending upon axon domain. More importantly, the current studies demonstrate little interruption of the ankG cytoskeleton acutely within the AIS, with its preservation out to 12h post-injury. Though qualitative in nature, these findings are consistent with previous quantitative evidence demonstrating the absence of a significant increase in ankG breakdown in the neocortex following cFPI in the rat [56] suggesting limited interruption of the AIS cytoskeleton following diffuse axonal. The retention of the cytoskeletal composition of the AIS has important implications for cell fate, as the loss ankG has been linked to a loss of neuronal polarity [23]. This retention of polarity is consistent with the regenerative response observed weeks to months following injury in this same model of mild TBI, whereby axon sprouting was observed to occur from the proximal axonal segment [20], a process requiring its continued molecular identification as the primary neurite/axon. Importantly, the retention of the AIS and neuronal polarity is also consistent with our recent electrophysiological studies performed using the same injury paradigm. The AIS and the channel and cytoskeleton components contained therein, are known to play an important role in regulation of intrinsic

NIH-PA Author Manuscript

NIH-PA Author Manuscript

NIH-PA Author Manuscript

neuronal excitability [5, 22, 28, 31]. We have recently demonstrated that following TAI, the *F–I* slope and the rheobase, two measures of intrinsic excitability, are initially depressed yet recover some normal properties by 2d post-injury [21]. Notably, others have demonstrated that pathological alterations in AIS morphology have in fact been found to result in changes in neuronal excitability [32]. Importantly the subtle injury-induced alterations in the AIS noted in the current manuscript are consistent with the plastic responses of the AIS, such as decreased length, which has been observed following ischemic [24] or blast [2] insults, and suggests the possibility of a temporary but incomplete disruption the AIS cytoskeleton following diffuse brain injury and a delayed restoration of neuronal excitability. These studies demonstrated a decrease in the length of the ankG cytoskeleton within the AIS following CNS injury. Although our current observations demonstrate the integrity of the AIS cytoskeleton within the first 12h quantitative analyses are needed to establish whether similar or perhaps more subtler effects upon AIS length are occurring following mild TBI.

In summary, the current communication reports the unique susceptibility of the AIS of neocortical neurons to injury during diffuse TBI. Additionally, we report the rapid disconnection of a significant percentage of injured axons, and demonstrate the localization of APP^+ swelling to the site of eventual axon disconnection. Notably the majority of swellings occurred within the AIS, yet, these occurred without significant disruption of the underlying cytoskeleton, consistent with the maintenance of neuronal polarity and restoration of neuronal excitability. Though the mechanisms responsible for both the initiation of axonal injury and the secondary cascade within the AIS are unknown, the unique structure of the AIS, both in ion channel and ECM composition, suggests the potential for pathological alterations that are unique to this domain. These issues warrant further investigation and may become the focus of future therapeutic manipulations targeting prevention of secondary injury and/or any subsequent neuroplastic response.

Acknowledgments

The authors would like to thank C. Lynn Davis, Jesse Sims and Sue Walker for their technical support. Funding provided by NIH grants NS077675 and NS047463.

Microscopy was performed at the VCU Department of Anatomy and Neurobiology Microscopy Facility, supported, in part, with funding from NIH-NINDS Center core grant (5P30NS047463-02).

References

1. Adams JH, Doyle D, Ford I, Gennarelli TA, Graham DI, McLellan DR. Diffuse axonal injury in head injury: definition, diagnosis and grading. Histopathology. 1989; 15(1):49–59. [PubMed: 2767623]
2. Baalman KL, Cotton RJ, Rasband SN, Rasband MN. Blast wave exposure impairs memory and decreases axon initial segment length. J Neurotrauma. 2013
3. Banik NL, Matzelle DC, Gantt-Wilford G, Osborne A, Hogan EL. Increased calpain content and progressive degradation of neurofilament protein in spinal cord injury. Brain Res. 1997; 752(1–2): 301–306. [PubMed: 9106471]
4. Bazarian JJ, Zhong J, Blyth B, Zhu T, Kavcic V, Peterson D. Diffusion tensor imaging detects clinically important axonal damage after mild traumatic brain injury: a pilot study. J Neurotrauma. 2007; 24(9):1447–1459. [PubMed: 17892407]
5. Bender KJ, Trussell LO. The physiology of the axon initial segment. Annu Rev Neurosci. 2012; 35:249–265. [PubMed: 22443507]
6. Bigler ED, Bazarian JJ. Diffusion tensor imaging: a biomarker for mild traumatic brain injury? Neurology. 2010; 74(8):626–627. [PubMed: 20107137]
7. Bisby MA, Bulger VT. Reversal of axonal transport at a nerve crush. J Neurochem. 1977; 29(2): 313–320. [PubMed: 69682]

NIH-PA Author Manuscript

NIH-PA Author Manuscript

NIH-PA Author Manuscript

8. Blumbergs PC, Scott G, Manavis J, Wainwright H, Simpson DA, McLean AJ. Staining of amyloid precursor protein to study axonal damage in mild head injury. Lancet. 1994; 344(8929):1055–1056. [PubMed: 7523810]
9. Bramlett HM, Kraydieh S, Green EJ, Dietrich WD. Temporal and regional patterns of axonal damage following traumatic brain injury: a beta-amyloid precursor protein immunocytochemical study in rats. J Neuropathol Exp Neurol. 1997; 56(10):1132–1141. [PubMed: 9329457]
10. Buki A, Farkas O, Doczi T, Povlishock JT. Preinjury administration of the calpain inhibitor MDL-28170 attenuates traumatically induced axonal injury. J Neurotrauma. 2003; 20(3):261–268. [PubMed: 12820680]
11. Buki A, Koizumi H, Povlishock JT. Moderate posttraumatic hypothermia decreases early calpain-mediated proteolysis and concomitant cytoskeletal compromise in traumatic axonal injury. Exp Neurol. 1999; 159(1):319–328. [PubMed: 10486200]
12. Buki A, Siman R, Trojanowski JQ, Povlishock JT. The role of calpain-mediated spectrin proteolysis in traumatically induced axonal injury. J Neuropathol Exp Neurol. 1999; 58(4):365–375. [PubMed: 10218632]
13. Carter LM, Starkey ML, Akrimi SF, Davies M, Mcmahon SB, Bradbury EJ. The Yellow Fluorescent Protein (YFP-H) mouse reveals neuroprotection as a novel mechanism underlying chondroitinase ABC-mediated repair after spinal cord injury. J Neurosci. 2008; 28(52):14107–14120. [PubMed: 19109493]
14. Dixon CE, Lyeth BG, Povlishock JT, Findling RL, Hamm RJ, Marmarou A, Young HF, Hayes RL. A fluid percussion model of experimental brain injury in the rat. J Neurosurg. 1987; 67(1): 110–119. [PubMed: 3598659]
15. Duflocq A, Chareyre F, Giovannini M, Couraud F, Davenne M. Characterization of the axon initial segment (AIS) of motor neurons and identification of a para-AIS and a juxtapara-AIS, organized by protein 4.1B. BMC Biol. 2011; 9:66. [PubMed: 21958379]
16. Erb DE, Povlishock JT. Axonal damage in severe traumatic brain injury: an experimental study in cat. Acta Neuropathol. 1988; 76(4):347–358. [PubMed: 2459896]
17. Feng G, Mellor RH, Bernstein M, Keller-Peck C, Nguyen QT, Wallace M, Nerbonne JM, Lichtman JW, Sanes JR. Imaging neuronal subsets in transgenic mice expressing multiple spectral variants of GFP. Neuron. 2000; 28(1):41–51. [PubMed: 11086982]
18. Gennarelli TA, Thibault LE, Tipperman R, Tomei G, Sergot R, Brown M, Maxwell WL, Graham DI, Adams JH, Irvine A. Axonal injury in the optic nerve: a model simulating diffuse axonal injury in the brain. J Neurosurg. 1989; 71(2):244–253. [PubMed: 2746348]
19. Gentleman SM, Nash MJ, Sweeting CJ, Graham DI. β-Amyloid precursor protein (βAPP) as a marker for axonal injury after head injury. Neuroscience Letters. 1993; 160(2):139–144. [PubMed: 8247344]
20. Greer JE, McGinn MJ, Povlishock JT. Diffuse traumatic axonal injury in the mouse induces atrophy, c-Jun activation, and axonal outgrowth in the axotomized neuronal population. J Neurosci. 2011; 31(13):5089–5105. [PubMed: 21451046]
21. Greer JE, Povlishock JT, Jacobs KM. Electrophysiological abnormalities in both axotomized and nonaxotomized pyramidal neurons following mild traumatic brain injury. J Neurosci. 2012; 32(19):6682–6687. [PubMed: 22573690]
22. Grubb MS, Burrone J. Activity-dependent relocation of the axon initial segment fine-tunes neuronal excitability. Nature. 2010; 465(7301):1070–1074. [PubMed: 20543823]
23. Hedstrom KL, Ogawa Y, Rasband MN. AnkyrinG is required for maintenance of the axon initial segment and neuronal polarity. J Cell Biol. 2008; 183(4):635–640. [PubMed: 19001126]
24. Hinman JD, Rasband MN, Carmichael ST. Remodeling of the axon initial segment after focal cortical and white matter stroke. Stroke. 2013; 44(1):182–189. [PubMed: 23233385]
25. Huh JW, Franklin MA, Widing AG, Raghupathi R. Regionally distinct patterns of calpain activation and traumatic axonal injury following contusive brain injury in immature rats. Dev Neurosci. 2006; 28(4–5):466–476. [PubMed: 16943669]
26. Inglese M, Makani S, Johnson G, Cohen BA, Silver JA, Gonen O, Grossman RI. Diffuse axonal injury in mild traumatic brain injury: a diffusion tensor imaging study. J Neurosurg. 2005; 103(2): 298–303. [PubMed: 16175860]

NIH-PA Author Manuscript

NIH-PA Author Manuscript

NIH-PA Author Manuscript

27. Iwata A, Stys PK, Wolf JA, Chen X-H, Taylor AG, Meaney DF, Smith DH. Traumatic axonal injury induces proteolytic cleavage of the voltage-gated sodium channels modulated by tetrodotoxin and protease inhibitors. J Neurosci. 2004; 24(19):4605–4613. [PubMed: 15140932]

28. Kaphzan H, Buffington SA, Jung JI, Rasband MN, Klann E. Alterations in intrinsic membrane properties and the axon initial segment in a mouse model of Angelman syndrome. J Neurosci. 2011; 31(48):17637–17648. [PubMed: 22131424]

29. Kelley BJ, Farkas O, Lifshitz J, Povlishock JT. Traumatic axonal injury in the perisomatic domain triggers ultrarapid secondary axotomy and Wallerian degeneration. Exp Neurol. 2006; 198(2):350–360. [PubMed: 16448652]

30. Kelley BJ, Lifshitz J, Povlishock JT. Neuroinflammatory responses after experimental diffuse traumatic brain injury. J Neuropathol Exp Neurol. 2007; 66(11):989–1001. [PubMed: 17984681]

31. Kole MHP, Stuart GJ. Signal processing in the axon initial segment. Neuron. 2012; 73(2):235–247. [PubMed: 22284179]

32. Kuba H. Structural tuning and plasticity of the axon initial segment in auditory neurons. J Physiol (Lond). 2012; 590(Pt 22):5571–5579. [PubMed: 23027822]

33. Lafrenaye AD, McGinn MJ, Povlishock JT. Increased intracranial pressure after diffuse traumatic brain injury exacerbates neuronal somatic membrane poration but not axonal injury: evidence for primary intracranial pressure-induced neuronal perturbation. J Cereb Blood Flow Metab. 2012; 32(10):1919–1932. [PubMed: 22781336]

34. Lewén A, Li GL, Nilsson P, Olsson Y, Hillered L. Traumatic brain injury in rat produces changes of beta-amyloid precursor protein immunoreactivity. Neuroreport. 1995; 6(2):357–360. [PubMed: 7756628]

35. Lewis SB, Finnie JW, Blumbergs PC, Scott G, Manavis J, Brown C, Reilly PL, Jones NR, McLean AJ. A head impact model of early axonal injury in the sheep. J Neurotrauma. 1996; 13(9):505–514. [PubMed: 8913967]

36. Li GL, Farooque M, Holtz A, Olsson Y. Changes of beta-amyloid precursor protein after compression trauma to the spinal cord: an experimental study in the rat using immunohistochemistry. J Neurotrauma. 1995; 12(3):269–277. [PubMed: 7473801]

37. Lifshitz J, Kelley BJ, Povlishock JT. Perisomatic thalamic axotomy after diffuse traumatic brain injury is associated with atrophy rather than cell death. J Neuropathol Exp Neurol. 2007; 66(3): 218–229. [PubMed: 17356383]

38. Lipton ML, Gellella E, Lo C, Gold T, Ardekani BA, Shifteh K, Bello JA, Branch CA. Multifocal white matter ultrastructural abnormalities in mild traumatic brain injury with cognitive disability: a voxel-wise analysis of diffusion tensor imaging. J Neurotrauma. 2008; 25(11):1335–1342. [PubMed: 19061376]

39. Lipton ML, Gulko E, Zimmerman ME, Friedman BW, Kim M, Gellella E, Gold T, Shifteh K, Ardekani BA, Branch CA. Diffusion-tensor imaging implicates prefrontal axonal injury in executive function impairment following very mild traumatic brain injury. Radiology. 2009; 252(3):816–824. [PubMed: 19567646]

40. Mac Donald CL, Dikranian K, Bayly P, Holtzman D, Brody D. Diffusion tensor imaging reliably detects experimental traumatic axonal injury and indicates approximate time of injury. J Neurosci. 2007; 27(44):11869–11876. [PubMed: 17978027]

41. Martz D, Garner J, Lasek RJ. Protein changes during anterograde-to-retrograde conversion of axonally transported vesicles. Brain Res. 1989; 476(1):199–203. [PubMed: 2464419]

42. Maxwell WL. Histopathological changes at central nodes of Ranvier after stretch-injury. Microsc Res Tech. 1996; 34(6):522–535. [PubMed: 8842021]

43. Maxwell WL, Graham DI. Loss of axonal microtubules and neurofilaments after stretch-injury to guinea pig optic nerve fibers. J Neurotrauma. 1997; 14(9):603–614. [PubMed: 9337123]

44. Maxwell WL, Irvine A, Graham, Adams JH, Gennarelli TA, Tipperman R, Sturatis M. Focal axonal injury: the early axonal response to stretch. J Neurocytol. 1991; 20(3):157–164. [PubMed: 1709964]

45. Maxwell WL, Kosanlavit R, McCreath BJ, Reid O, Graham DI. Freeze-fracture and cytochemical evidence for structural and functional alteration in the axolemma and myelin sheath of adult

NIH-PA Author Manuscript

NIH-PA Author Manuscript

NIH-PA Author Manuscript

guinea pig optic nerve fibers after stretch injury. J Neurotrauma. 1999; 16(4):273–284. [PubMed: 10225214]

46. McGinn MJ, Kelley BJ, Akinyi L, Oli MW, Liu MC, Hayes RL, Wang KKW, Povlishock JT. Biochemical, structural, and biomarker evidence for calpain-mediated cytoskeletal change after diffuse brain injury uncomplicated by contusion. J Neuropathol Exp Neurol. 2009; 68(3):241–249. [PubMed: 19225412]
47. McKenzie KJ, McLellan DR, Gentleman SM, Maxwell WL, Gennarelli TA, Graham DI. Is beta-APP a marker of axonal damage in short-surviving head injury? Acta Neuropathol. 1996; 92(6): 608–613. [PubMed: 8960319]
48. Oehmichen M, Theuerkauf I, Meissner C. Is traumatic axonal injury (AI) associated with an early microglial activation? Application of a double-labeling technique for simultaneous detection of microglia and AI. Acta Neuropathol. 1999; 97(5):491–494. [PubMed: 10334486]
49. Pettus EH, Povlishock JT. Characterization of a distinct set of intra-axonal ultrastructural changes associated with traumatically induced alteration in axolemmal permeability. Brain Res. 1996; 722(1–2):1–11. [PubMed: 8813344]
50. Pettus EH, Christman CW, Giebel ML, Povlishock JT. Traumatically induced altered membrane permeability: its relationship to traumatically induced reactive axonal change. J Neurotrauma. 1994; 11(5):507–522. [PubMed: 7861444]
51. Povlishock JT, Becker DP, Cheng CL, Vaughan GW. Axonal change in minor head injury. J Neuropathol Exp Neurol. 1983; 42(3):225–242. [PubMed: 6188807]
52. Povlishock JT, Buki A, Koiziumi H, Stone J, Okonkwo DO. Initiating mechanisms involved in the pathobiology of traumatically induced axonal injury and interventions targeted at blunting their progression. Acta Neurochir Suppl. 1999; 73:15–20. [PubMed: 10494336]
53. Povlishock JT, Marmarou A, McIntosh T, Trojanowski JQ, Moroi J. Impact acceleration injury in the rat: evidence for focal axolemmal change and related neurofilament sidearm alteration. J Neuropathol Exp Neurol. 1997; 56(4):347–359. [PubMed: 9100665]
54. Povlishock JT, Katz DI. Update of neuropathology and neurological recovery after traumatic brain injury. J Head Trauma Rehabil. 2005; 20(1):76–94. [PubMed: 15668572]
55. Rasband MN. Composition, assembly, and maintenance of excitable membrane domains in myelinated axons. Semin Cell Dev Biol. 2011; 22(2):178–184. [PubMed: 20932927]
56. Reeves TM, Greer JE, Vanderveer AS, Phillips LL. Proteolysis of submembrane cytoskeletal proteins ankyrin-G and αII-spectrin following diffuse brain injury: a role in white matter vulnerability at Nodes of Ranvier. Brain Pathol. 2010; 20(6):1055–1068. [PubMed: 20557305]
57. Reyn von CR, Mott RE, Siman R, Smith DH, Meaney DF. Mechanisms of calpain mediated proteolysis of voltage gated sodium channel α-subunits following in vitro dynamic stretch injury. J Neurochem. 2012; 121(5):793–805. [PubMed: 22428606]
58. Reyn von CR, Spaethling JM, Mesfin MN, Ma M, Neumar RW, Smith DH, Siman R, Meaney DF. Calpain mediates proteolysis of the voltage-gated sodium channel alpha-subunit. J Neurosci. 2009; 29(33):10350–10356. [PubMed: 19692609]
59. Rutgers DR, Fillard P, Paradot G, Tadié M, Lasjaunias P, Ducreux D. Diffusion tensor imaging characteristics of the corpus callosum in mild, moderate, and severe traumatic brain injury. AJNR Am J Neuroradiol. 2008; 29(9):1730–1735. [PubMed: 18617586]
60. Saatman KE, Abai B, Grosvenor A, Vorwerk CK, Smith DH, Meaney DF. Traumatic axonal injury results in biphasic calpain activation and retrograde transport impairment in mice. J Cereb Blood Flow Metab. 2003; 23(1):34–42. [PubMed: 12500089]
61. Sahenk Z, Lasek RJ. Inhibition of proteolysis blocks anterograde-retrograde conversion of axonally transported vesicles. Brain Res. 1988; 460(1):199–203. [PubMed: 2464405]
62. Schafer DP, Jha S, Liu F, Akella T, McCullough LD, Rasband MN. Disruption of the axon initial segment cytoskeleton is a new mechanism for neuronal injury. J Neurosci. 2009; 29(42):13242–13254. [PubMed: 19846712]
63. Schumacher PA, Siman RG, Fehlings MG. Pretreatment with calpain inhibitor CEP-4143 inhibits calpain I activation and cytoskeletal degradation, improves neurological function, and enhances axonal survival after traumatic spinal cord injury. J Neurochem. 2000; 74(4):1646–1655. [PubMed: 10737623]

NIH-PA Author Manuscript

NIH-PA Author Manuscript

NIH-PA Author Manuscript

64. Serbest G, Burkhardt MF, Siman R, Raghupathi R, Saatman KE. Temporal profiles of cytoskeletal protein loss following traumatic axonal injury in mice. Neurochem Res. 2007; 32(12):2006–2014. [PubMed: 17401646]

65. Sherriff FE, Bridges LR, Sivaloganathan S. Early detection of axonal injury after human head trauma using immunocytochemistry for beta-amyloid precursor protein. Acta Neuropathol. 1994; 87(1):55–62. [PubMed: 8140894]

66. Sherriff FE, Bridges LR, Gentleman SM, Sivaloganathan S, Wilson S. Markers of axonal injury in post mortem human brain. Acta Neuropathol. 1994; 88(5):433–439. [PubMed: 7847072]

67. Sidaros A, Engberg AW, Sidaros K, Liptrot MG, Herning M, Petersen P, Paulson OB, Jernigan TL, Rostrup E. Diffusion tensor imaging during recovery from severe traumatic brain injury and relation to clinical outcome: a longitudinal study. Brain. 2008; 131(Pt 2):559–572. [PubMed: 18083753]

68. Singleton RH, Povlishock JT. Identification and characterization of heterogeneous neuronal injury and death in regions of diffuse brain injury: evidence for multiple independent injury phenotypes. J Neurosci. 2004; 24(14):3543–3553. [PubMed: 15071102]

69. Singleton RH, Zhu J, Stone JR, Povlishock JT. Traumatically induced axotomy adjacent to the soma does not result in acute neuronal death. J Neurosci. 2002; 22(3):791–802. [PubMed: 11826109]

70. Smith DH, Hicks R, Povlishock JT. Therapy Development for Diffuse Axonal Injury. J Neurotrauma. 2013; 30(5):307–323. [PubMed: 23252624]

71. Smith DH, Meaney DF, Shull WH. Diffuse axonal injury in head trauma. J Head Trauma Rehabil. 2003; 18(4):307–316. [PubMed: 16222127]

72. Smith RS, Snyder RE. Reversal of rapid axonal transport at a lesion: leupeptin inhibits reversed protein transport, but does not inhibit reversed organelle transport. Brain Res. 1991; 552(2):215–227. [PubMed: 1717113]

73. Snyder RE, Smith RS, Chen X. Reversal of rapidly transported protein and organelles at an axonal lesion. Brain Res. 1994; 635(1–2):49–58. [PubMed: 8173979]

74. Stone JR, Singleton RH, Povlishock JT. Antibodies to the C-terminus of the β-amyloid precursor protein (APP): a site specific marker for the detection of traumatic axonal injury. Brain Res. 2000; 871(2):288–302. [PubMed: 10899295]

75. Sugino K, Hempel CM, Miller MN, Hattox AM, Shapiro P, Wu C, Huang ZJ, Nelson SB. Molecular taxonomy of major neuronal classes in the adult mouse forebrain. Nat Neurosci. 2006; 9(1):99–107. [PubMed: 16369481]

76. Wang J, Hamm RJ, Povlishock JT. Traumatic axonal injury in the optic nerve: evidence for axonal swelling, disconnection, dieback, and reorganization. J Neurotrauma. 2011; 28(7):1185–1198. [PubMed: 21506725]

77. Wolf JA, Stys PK, Lusardi T, Meaney D, Smith DH. Traumatic axonal injury induces calcium influx modulated by tetrodotoxin-sensitive sodium channels. J Neurosci. 2001; 21(6):1923–1930. [PubMed: 11245677]

78. Yuh EL, Mukherjee P, Lingsma HF, Yue JK. Magnetic resonance imaging improves 3- month outcome prediction in mild traumatic brain injury. Ann Neurol. 2012

NIH-PA Author Manuscript
NIH-PA Author Manuscript
NIH-PA Author Manuscript

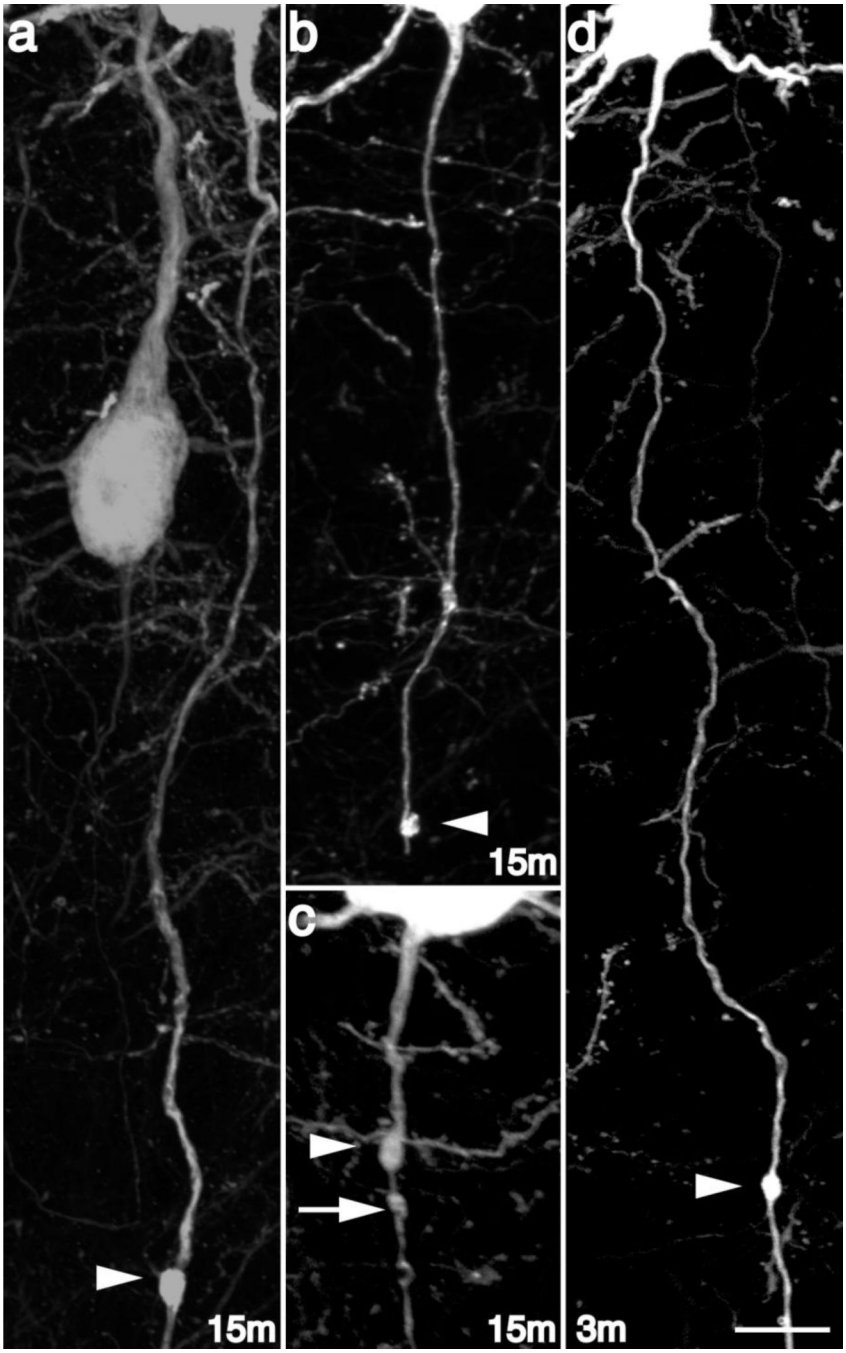

Fig 1. Diffuse brain injury induces rapid secondary axotomy within Layer V pyramidal neurons

Following cFPI, the YFP^+ axonal swellings (arrowheads) were evident as early as 15m post injury (a–c). Several injured YFP^+ fibers at this time point following injury showed clear evidence for disconnection (b), though many demonstrated retained axonal continuity (a, c). Additionally, YFP^+ swellings could be found at various sites along the YFP^+ axon, both distal (a, b) and proximal (c) relative to the cell body of origin. Note the presence of multiple swellings along the length of some injured YFP^+ fibers at this early time point (C, arrow/arrowheads). Importantly, axonal disconnection (b) at 15m following injury was the result of secondary and progressive axonal change, as limited axonal alterations were observed at 3–

4m following injury, and the only YFP^+ swelling noted remained in continuity with the distal axonal segment (d). Scale: 10 μm

NIH-PA Author Manuscript
NIH-PA Author Manuscript
NIH-PA Author Manuscript

NIH-PA Author Manuscript
NIH-PA Author Manuscript
NIH-PA Author Manuscript

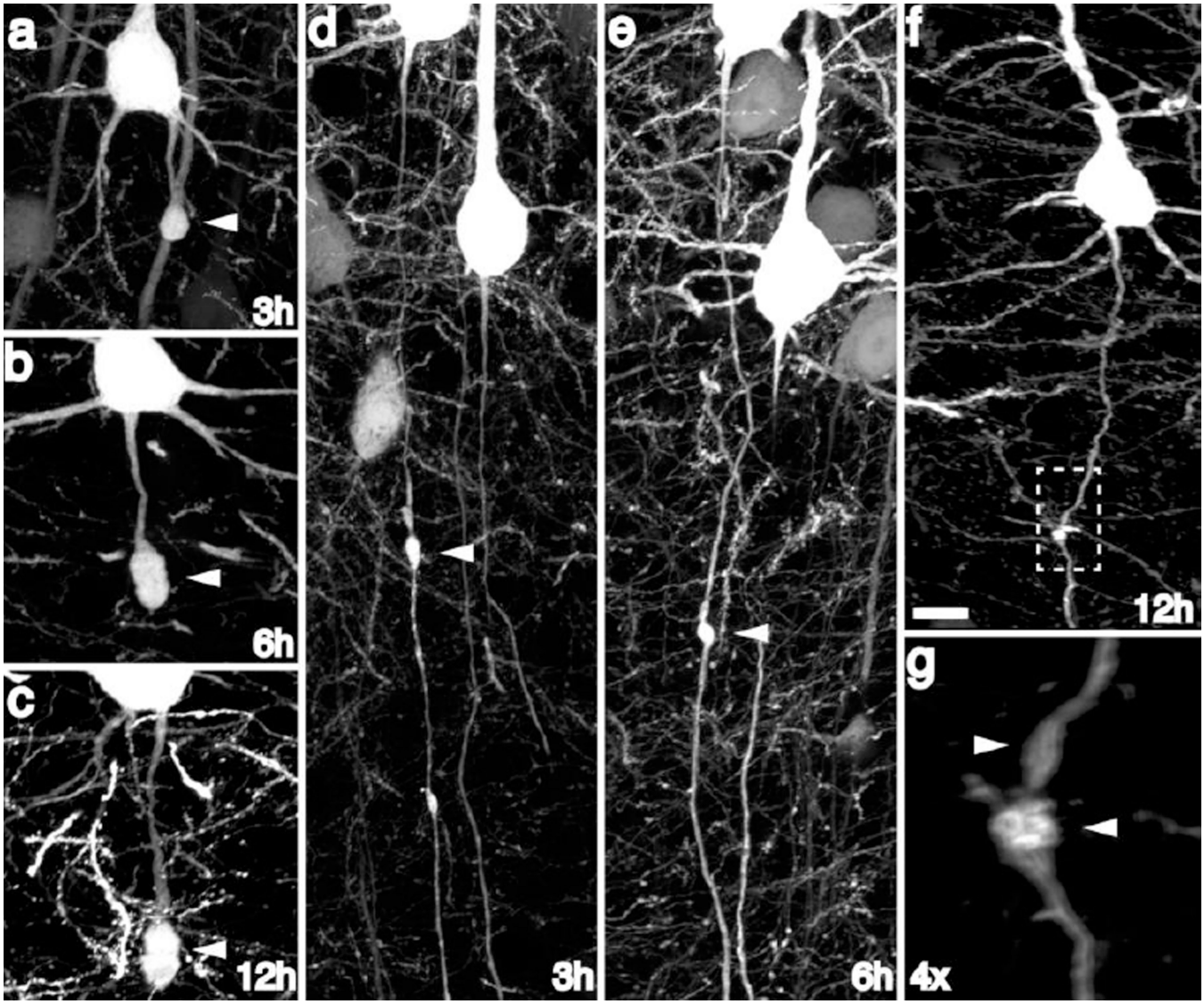

Fig 2. YFP$^+$ axonal swellings progressively enlarge and disconnect over time post-injury

Consistent with progressive axonal change, YFP$^+$ swellings continue to enlarge over the next 12h post-injury (a–c). Though the majority of swellings progress to disconnection over this 12h time span, occasional swellings still maintaining axonal continuity could be found at later time points following injury (d–g), underscoring a temporally heterogeneous evolution of YFP$^+$ swellings over time. Scale: 10 μm

NIH-PA Author Manuscript
NIH-PA Author Manuscript
NIH-PA Author Manuscript

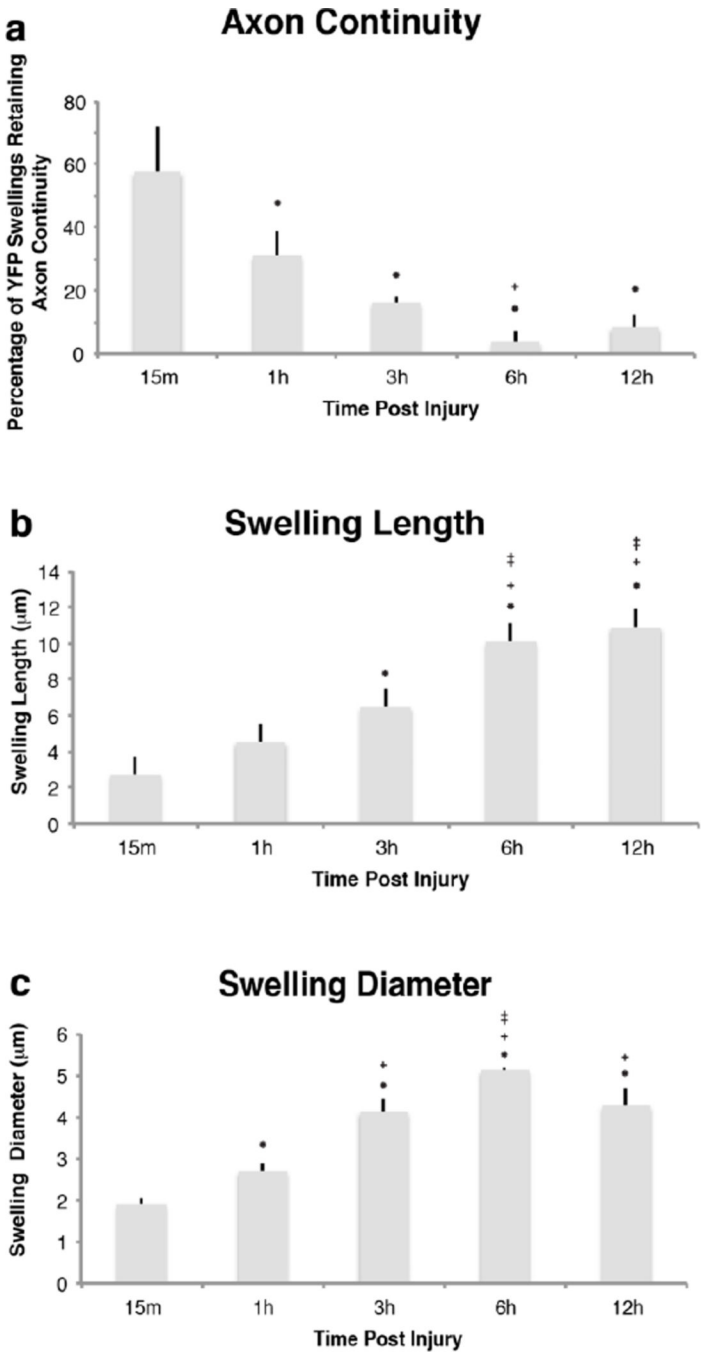

Fig 3. Quantitative assessment of the temporal alteration in YFP$^+$ swelling characteristics revealed rapid axonal disconnection following TAI

When quantified, a large number of injured axons demonstrated axonal disconnection at 15m post-injury (a). Reflecting progressive disconnection, the number of YFP$^+$ axons demonstrating axonal continuity decreased significantly at 1h, 3h and 6h when compared to 15m post-injury, with most fibers demonstrating disconnection by 6h post-injury (a). Quantitative analysis of YFP$^+$ swellings revealed significant increases in YFP$^+$ swelling length (b) and diameter (c), reflecting progressive swelling enlargement over time. Importantly, (* $p < 0.05$, compared to 15m; + $p < 0.05$, compared to 1h; ± $p < 0.05$, compared to 3h)

NIH-PA Author Manuscript
NIH-PA Author Manuscript
NIH-PA Author Manuscript

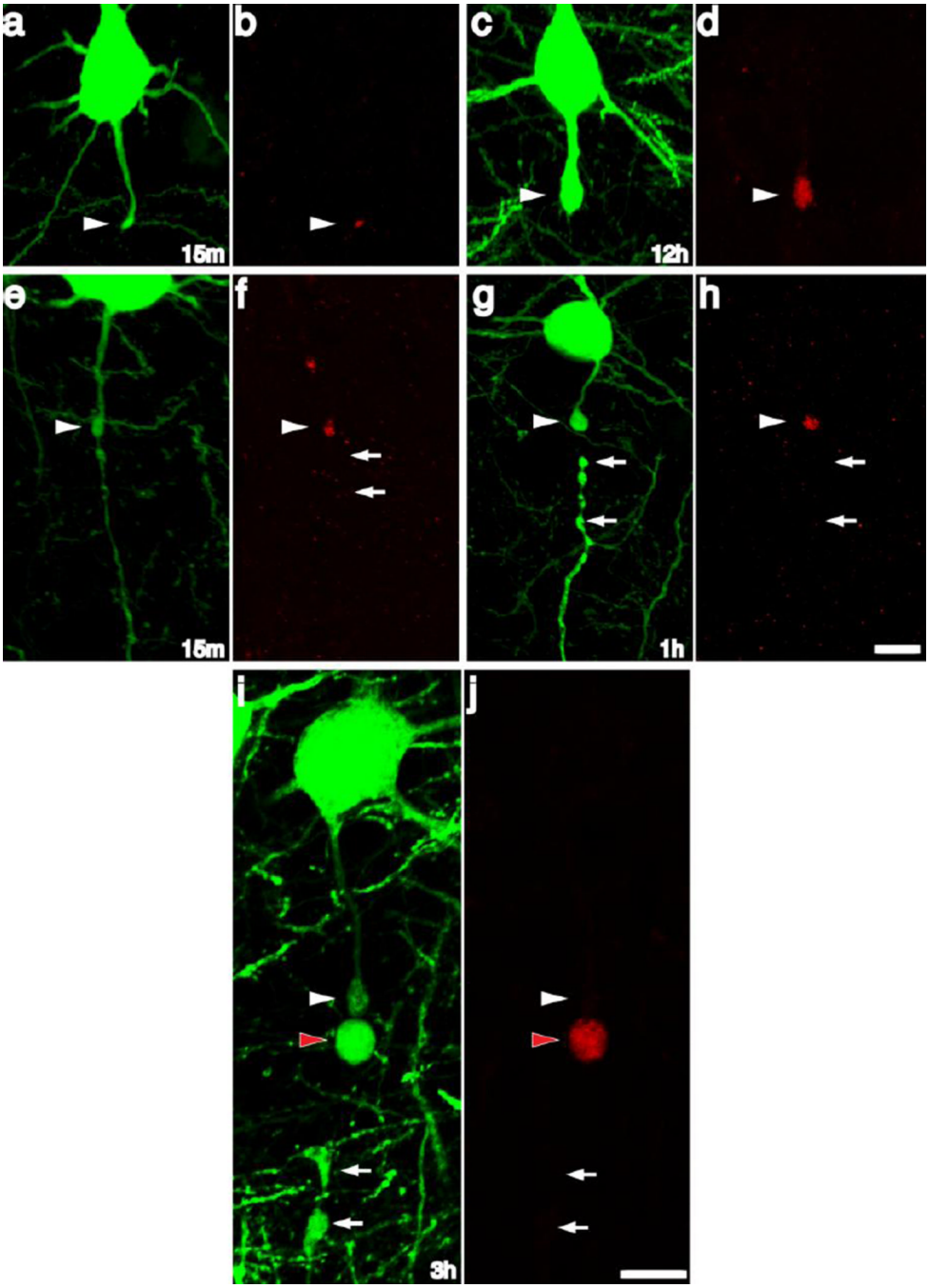

Fig 4. β-Amyloid precursor protein accumulation marks the site of eventual axon disconnection

At 15m following injury APP^{+}/YFP^{+} swellings could be identified within the neocortex (a, b, e, f). Within axons maintaining continuity, APP was consistently observed to be present in the more proximal swellings (e, f arrowheads) and typically excluded from more distal swellings (e, f arrows). Additional APP accumulation occurred within the larger YFP^{+} swellings at later time points (c, d). Importantly, as axons disconnected at later time points (f, g) APP localization remained consistent with that observed at 15m. Note the disconnected YFP^{+} axon, demonstrating APP immunoreactivity within the proximal YFP^{+} swelling (f, g arrowhead) with a lack of similar immunoreactivity within distal swellings (f, g arrows). Importantly, at later time points (i–j) were multiple swellings were found within

disconnected axons, APP immunoreactivity was restricted to the swelling adjacent to the site of disconnection, suggesting that the extent of APP accumulation along the length of an injured YFP^+ axon demarcates the region that will be retained following eventual disconnection. Scale: 10 μm

NIH-PA Author Manuscript
NIH-PA Author Manuscript
NIH-PA Author Manuscript

NIH-PA Author Manuscript
NIH-PA Author Manuscript
NIH-PA Author Manuscript

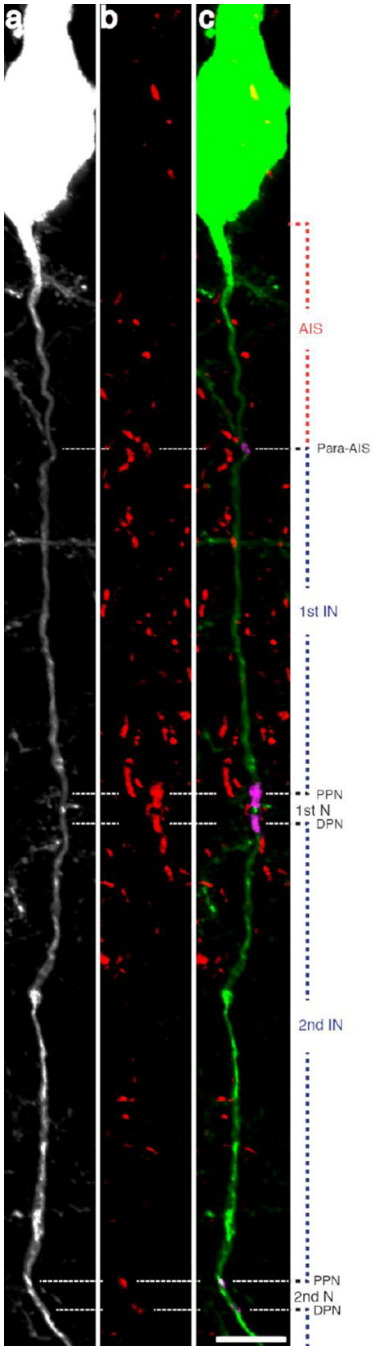

Fig 5. Caspr immunoreactivity demarcates multiple axon domains

Caspr immunoreactive bands located along YFP^{+} axons mark sites of axoglial interaction. Note the consistent pattern of immunoreactivity, with a proximal single band of Caspr immunoreactivity localized to the para-AIS and the beginning of myelination, delineating the more proximal AIS. More distal Caspr immunoreactivity appears with Caspr bands occurring in pairs, marking two adjacent paranodes, flanking the node of Ranvier. Scale: 10 μm

NIH-PA Author Manuscript
NIH-PA Author Manuscript
NIH-PA Author Manuscript

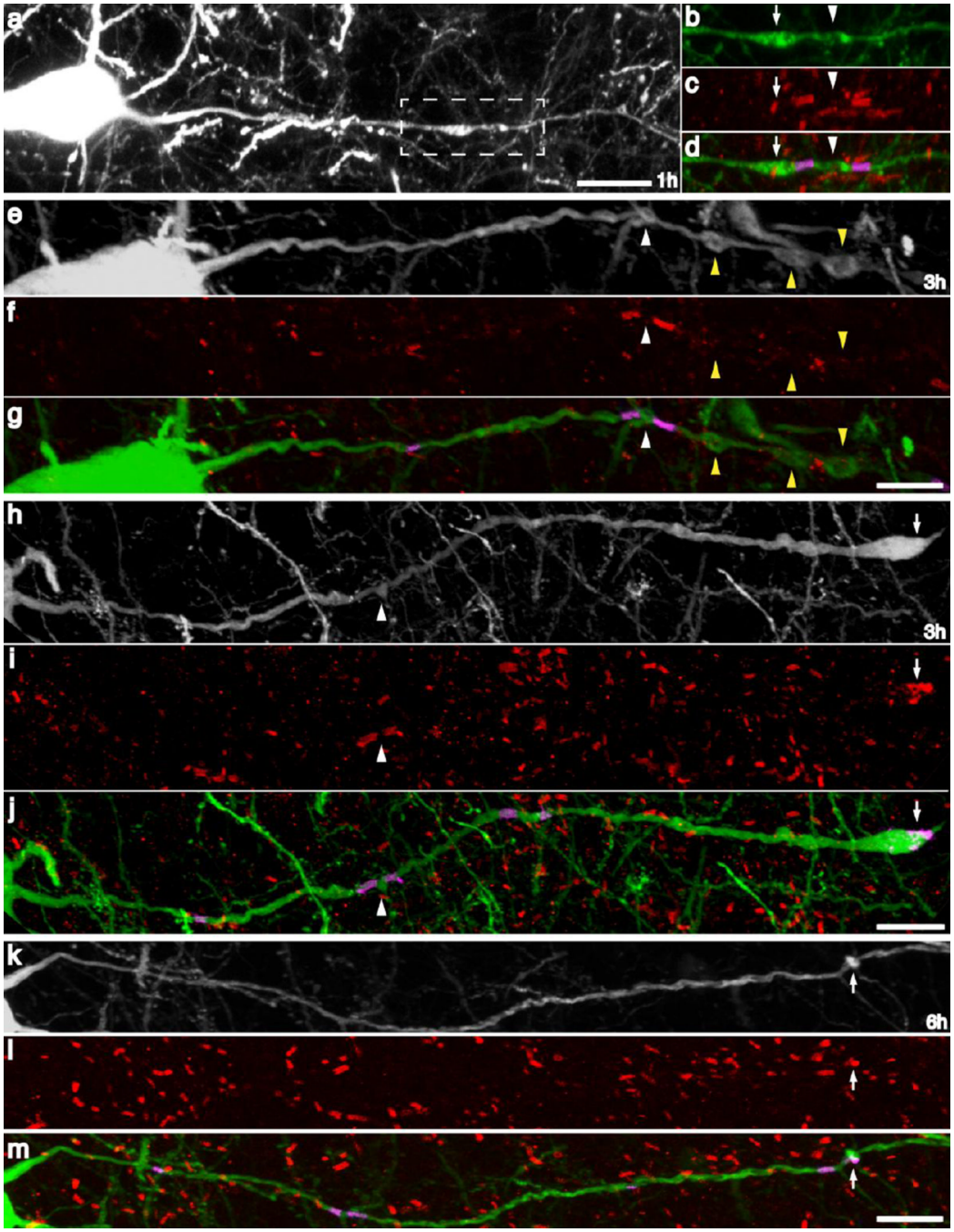

Fig 6. TAI occurs in all axon domains following cFPI

Utilizing Caspr immunoreactivity, YFP^+ swellings following injury were often localized to paranodal and nodal regions (a–d, h–j). Less frequently, swellings were observed within the intermodal region between two $Caspr^+$ nodal regions (e–g). At later time points, YFP^+ swellings, lacking continuity, were often observed to have maintained a $Caspr^+$ region within the distal region of the YFP^+ swelling (h–j), presumably indicating disconnection within the distal nodal region and retention of one $Caspr^+$ hemi node within the distal YFP^+ swelling. Additionally, paranodal YFP^+ swellings were also observed to occur without apparent morphological alteration of the adjacent nodal or internodal regions (k–m). Scale: 10 μm

NIH-PA Author Manuscript
NIH-PA Author Manuscript
NIH-PA Author Manuscript

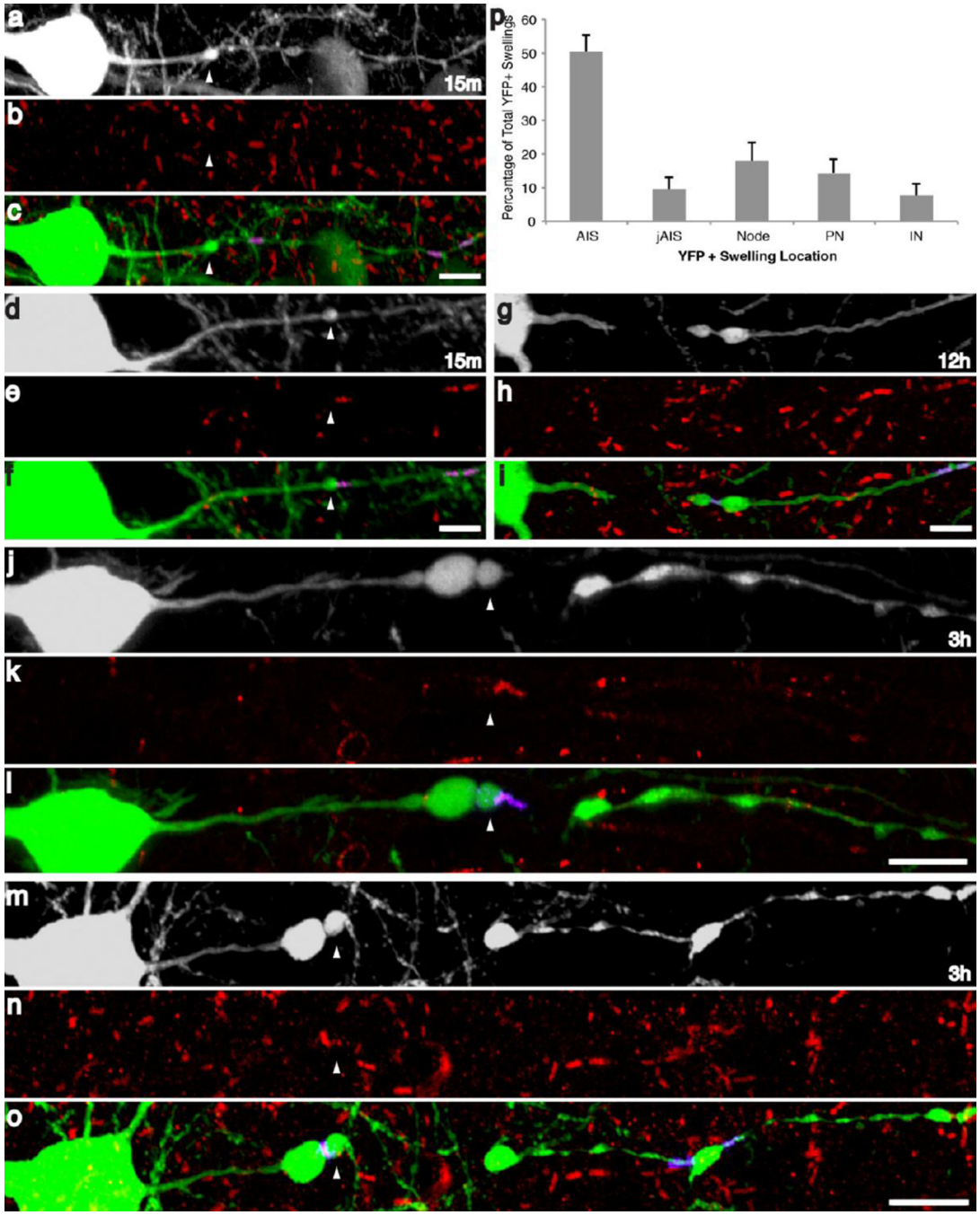

Fig 7. Axonal injury following cFPI preferentially occurs in the axon initial segment

Following quantitative analysis, the majority of YFP^+ axonal swellings were found to occur within the AIS (p). At 15m YFP^+ swellings were predominantly localized at the end of the AIS, proximal to the para-AIS (d–f), though several swellings were found to occur within the AIS (a–c). At later time points and following disconnection, swellings were observed within the AIS (white arrowheads, j–1), injured YFP^+ axons were often found to have retained Caspr immunoreactivity within the distal region of the swelling (j–o) or this $Caspr^+$ axoglial interaction was clearly visible within the distal, disconnected YFP axonal segment (G–I). Scale: 10 μm

NIH-PA Author Manuscript
NIH-PA Author Manuscript
NIH-PA Author Manuscript

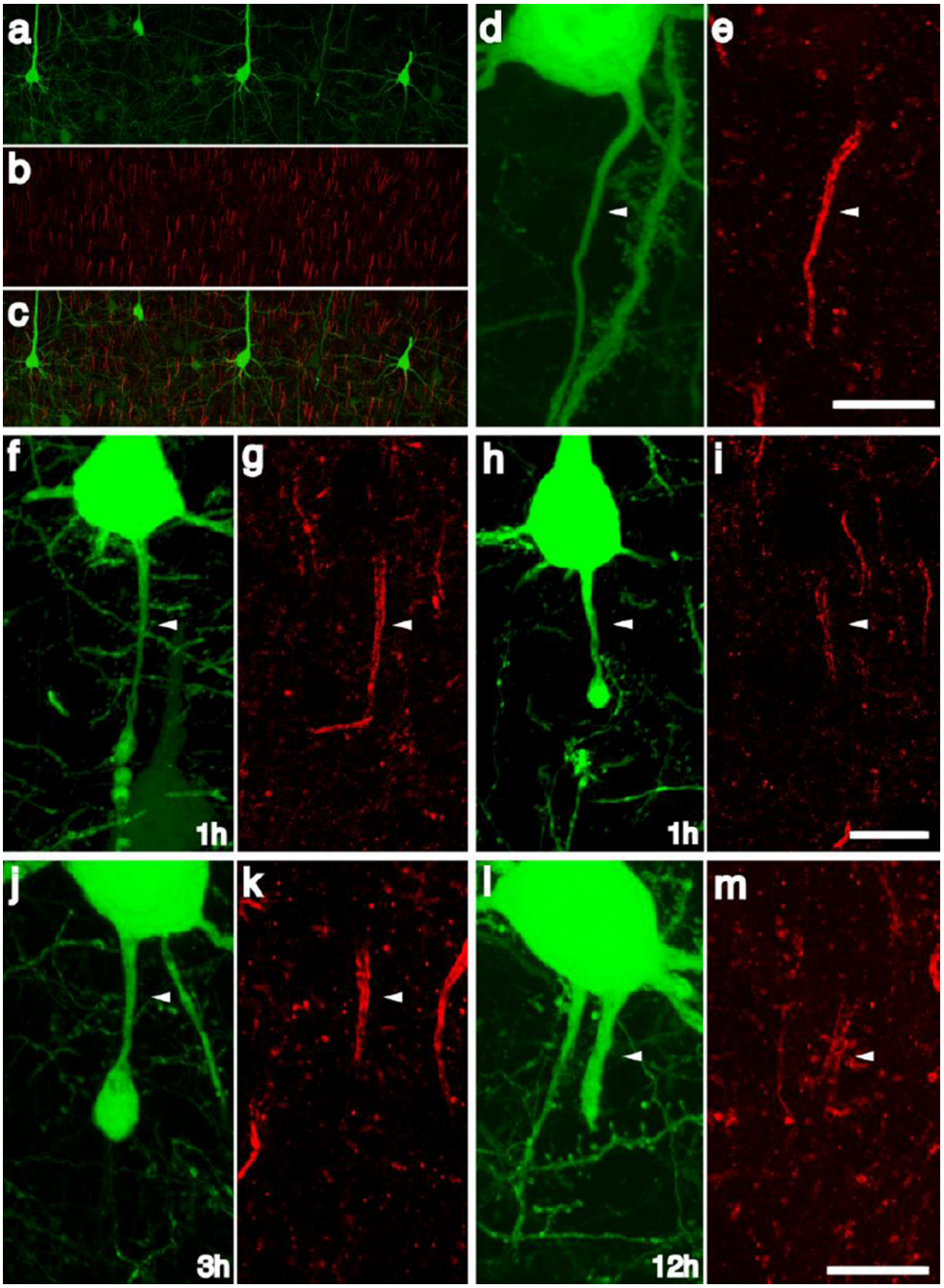

Fig 8. The AIS cytoskeletal integrity is conserved following traumatic axonal injury within the AIS

AnkG labeled the axon initial segments throughout the neocortex in sham-injured animals (a–c). Within intact axons of sham-injured and injured animals demonstrating no focal swellings, AnkG immunolabeling revealed a discrete and compact AIS associated with each YFP^+ neuron (d, e). Within most YFP^+ axons demonstrating swellings within the AIS, the AnkG cytoskeleton was conserved and consistent with the pattern observed within sham animals with loss of AnkG expression restricted to the region of axonal swelling (1h f, G; 3h j, k). Occasional axotomized neurons demonstrated attenuation of the AnkG expression within the AIS (h, i) and within YFP^+ axons demonstrating expansion of the swelling to

include the entire AIS ankG expression is still present directly underneath the plasmolemma (l, m). Scale: 10 μm

NIH-PA Author Manuscript
NIH-PA Author Manuscript
NIH-PA Author Manuscript